

GRAVITATIONAL COLLIDER PHYSICS VIA PULSAR-BLACK HOLE BINARIES II: FINE AND HYPERFINE STRUCTURES ARE FAVORED

XI TONG^{1,2}, YI WANG^{1,2}, AND HUI-YU ZHU^{1,2}

¹Department of Physics, The Hong Kong University of Science and Technology,
Clear Water Bay, Kowloon, Hong Kong, P.R.China and

²The HKUST Jockey Club Institute for Advanced Study, The Hong Kong University of Science and Technology,
Clear Water Bay, Kowloon, Hong Kong, P.R.China

Draft version July 13, 2021

Abstract

A rotating black hole can be clouded by light bosons via superradiance, and thus acquire an atom-like structure. If such a gravitational atom system is companioned with a pulsar, the pulsar can trigger transitions between energy levels of the gravitational atom, and these transitions can be detected by pulsar timing. We show that in such pulsar-black hole systems, fine and hyperfine structure transitions are more likely to be probed than the Bohr transition. Also, the calculation of these fine and hyperfine structure transitions are under better analytic control. Thus, these fine and hyperfine structure transitions are more ideal probes in the search for gravitational collider signals in pulsar-black hole systems.

1. Introduction

Compact objects play an important role in astrophysics and particle cosmology. With their astronomical mass squeezed into a compact region of spacetime, these objects provide an ideal platform for high energy astrophysical phenomena as well as a test ground for gravity (Shapiro and Teukolsky 1983; Camenzind 2007).

Arguably, the most notable of the compact objects are pulsars and black holes. Pulsars are usually rotating neutron stars that emit beams of electromagnetic radiation from their magnetic poles. The beam sweeps across the earth periodically due to the rotation. To a distant observer, despite its complex internal dynamics, a pulsar can be simply viewed as a clock that ticks by emitting periodic radio pulses. The precise periodicity of the pulsar makes it an excellent timing tool. For instance, pulsar timing is used to measure the orbital decay of binary systems (Hulse and Taylor 1975; Weisberg and Taylor 2004), to detect low-frequency Gravitational Waves (GWs) (Hobbs et al. 2010; Dewdney et al. 2009; Arzoumanian et al. 2020), to probe gravity in the strong-field regime (Angéil et al. 2010), and even to serve as autonomous space navigation beacons (Becker et al. 2013).

Black holes also play a central role in modern physics. Although isolated stationary black holes are classically characterized only by three parameters, they are known to carry more structures in the presence of perturbations (Konoplya and Zhidenko 2011; Hawking et al. 2016). Not only does the horizon emit Hawking radiation quantum mechanically (Hawking 1974), which inspired numerous studies on the long-standing information paradox (Hawking 1975), a rotating black hole carries a dissipative ergoregion capable of radiating particles on a classical level (Zel'Dovich 1971; Press and Teukolsky 1972). This phenomenon known as superradiance has also been widely studied for over half a century (see a comprehen-

sive review given by Brito et al. (2015b)). For bosonic particles with mass $\mu \lesssim (GM_B)^{-1}$, where M_B is the mass of the black hole, superradiance triggers an instability in the spectrum of the black hole bound states (Damour et al. 1976). This leads to the formation of a bosonic cloud of size $r_1 \sim \mathcal{O}(10^1-10^3)GM_B$ around the black hole, with an energy spectrum similar to that of the hydrogen atom. In isolation, such a gravitational atom emits monochromatic GWs through pair annihilations as well as spontaneous level transitions (Arvanitaki and Dubovsky 2011). When a binary companion is introduced, the periodic orbital motion may hit the resonance band of the gravitational atom and induce Landau-Zener transitions (Landau 1932; Zener 1932) between different energy levels. The backreaction effect produces floating or sinking/kicked orbits observable from the GW signatures emitted by the binary. This recently proposed framework aimed at probing ultralight bosons is known as Gravitational Collider Physics (GCP) (Baumann et al. 2019a,b, 2020).

However, GW (Ng et al. 2020) is not the only observation channel for GCP resonances and ultralight bosons. The backreaction on the binary can be naturally viewed as a change of orbital period derivative, *i.e.*, a timing problem. Given the simple yet accurate time periodicity of the pulsar, it is natural to consider the Pulsar-Black Hole (PSR-BH) binary as a viable probe of the GCP resonances. This PSR-BH-radio observation channel has recently been verified in (Ding et al. 2021) for Bohr transitions of the gravitational atom¹.

Bohr transitions change the principal quantum number, thus due to the narrow mass range of the pulsar, the corresponding resonance frequency is relatively high, and the orbital period can be as short as $P_r \sim \mathcal{O}(1)$ s. Hence the pulsar timing accuracy proves to be always sufficient. However, there are still several problems faced by the PSR-BH-radio channel for Bohr transitions. (i)

xtongac@connect.ust.hk
phyw@ust.hk
hzhuvav@connect.ust.hk

¹ See other PSR-BH approaches to ultralight bosons in (Kavic et al. 2020; Seymour and Yagi 2020).

The short binary period during Bohr transitions suggests that the binary is near the end of the inspiral process. Binaries with such a short period are statistically disfavored. Given the fact that the number of observable PSR-BH binaries in our Galaxy is limited (Faucher-Giguère and Loeb 2011; Shao and Li 2018; Chattopadhyay et al. 2020), the event rate for Bohr transitions in the PSR-BH binaries may be extremely low. (ii) During a Bohr transition, the binary separation is comparable to the size of the boson cloud. This may threaten the validity of the quadrupole approximation, leading to the inadequacy of considering a narrow resonance with $\Delta m = 2$ only. Additional effects such as dynamical friction (Zhang and Yang 2020), upscattering effects (Wong 2020), and the emergence of additional molecular states (Ikeda et al. 2021) may also dramatically change the prediction.

Compared to the Bohr transition, fine/hyperfine GCP transitions are observationally more probable and theoretically cleaner to analyze. In this work, we set out to analyze the fine/hyperfine GCP transitions of PSR-BH binaries for ultralight scalar bosons. The advantages of probing GCP with fine/hyperfine transition are: (i) The fine and hyperfine splittings are suppressed by extra factors of α^2 and α^3 respectively, where $\alpha \equiv GM_B\mu \ll 1$ is the gravitational fine structure constant. Therefore, they have a much longer resonance period. In addition, some fine/hyperfine transitions give floating orbits which enjoy an extremely long duration. This dramatically increases the event rate. (ii) The increase in resonance period is accompanied by the increase in the binary separation, which is now much greater than the cloud radius. This ensures the validity of the quadrupole approximation and the narrow resonance.

Apparently, a disadvantage of fine/hyperfine transitions is that the signal is weaker than Bohr transitions. The long orbital period gives rise to an orbital decay that may be too tiny to be detected by the first generation of space GW detectors (Amaro-Seoane et al. 2017; Luo et al. 2020; Mei et al. 2021; Ando et al. 2009). However, thanks to the well-established timing accuracy of pulsars, a long-term observation is sufficient to capture the fine/hyperfine resonances, as we will show below.

This paper is organized as follows. In Sect. 2, we review some technical details of the gravitational atom and GCP transitions. In Sect. 3, we discuss the problems faced by the Bohr transitions and motivate our study for fine/hyperfine transitions. Then in Sect. 4, we focus on the major fine/hyperfine transitions induced by the quadrupole moment of the orbiting pulsar and analyze their observational feasibility. We conclude and give future prospects in Sect. 5.

2. The Gravitational Atom

In this section, we briefly review the basic aspects of the gravitational atom and GCP following Baumann et al. (2019a) and Baumann et al. (2020). A Kerr black hole is equipped with a dissipative ergosphere that can amplify incoming waves (Penrose 1969; Zel'Dovich 1971). For a massive bosonic field, its mass serves as a natural mirror that reflects back the amplified modes (Press and Teukolsky 1972; Cardoso et al. 2004), from which an in-

stability is generated (Damour et al. 1976). This superradiance instability leads to the growth of a bosonic cloud, whose behavior is governed by the Schrödinger equation with corrections from Kerr spacetime,

$$i\partial_t\psi(t, \vec{x}) = \left(-\frac{1}{2\mu}\partial_{\vec{x}}^2 - \frac{\alpha}{r} + \mathcal{O}(\alpha^2)\right)\psi(t, \vec{x}), \quad (1)$$

where $\alpha \ll 1$ guarantees the validity of non-relativistic expansion. The solutions of the Schrödinger equation with in-going boundary condition at the horizon are atomic states $|nlm\rangle$ labeled by the principal, angular and magnetic quantum numbers². The frequency of each eigenstate is in general complex: $\omega_{nlm} = E_{nlm} + i\Gamma_{nlm}$, with

$$E_{nlm} = \mu \left(1 - \frac{\alpha^2}{2n^2} - \frac{\alpha^4}{8n^4} - \frac{(3n-2l-1)\alpha^4}{n^4(l+1/2)} + \frac{2\tilde{a}m\alpha^5}{n^3l(l+1/2)(l+1)} + \mathcal{O}(\alpha^6)\right), \quad (2)$$

and

$$\Gamma_{nlm} = 2\tilde{r}_+ C_{nlm}(m\Omega_H - \omega_{nlm})\alpha^{4l+5}, \quad (3)$$

where $\tilde{r} \equiv r/M_B$ and $\tilde{a} \equiv a/M_B \lesssim 1$ is the dimensionless black hole spin. For simplicity, we will assume $\tilde{a} \simeq 1$ throughout this work, since astrophysical BHs in binaries generally have a large spin (O'Shaughnessy et al. 2005; Nielsen 2016). C_{nlm} can be found in Baumann et al. (2019a). Notice that although (3) is derived under Detweiler's approximation (Detweiler 1980) with $\alpha \ll 1$, numerical studies have confirmed its validity for $\alpha < 0.5$ (Brito et al. 2015b). For a positive Γ_{nlm} , the total mass of the state M_{nlm} will grow at a timescale $T_{nlm}^{(\text{growth})} \equiv \Gamma_{nlm}^{-1}$ until saturation, then it slowly depletes via the emission of GWs. The depletion power of a highest helicity state with $l = m$ is

$$\dot{M}_{nlm} = -B_{nl} \left(\frac{M_{nlm}}{M_B}\right)^2 \alpha^{4l+10}. \quad (4)$$

The coefficient B_{nl} is computed by Yoshino and Kodama (2014) in the flat spacetime limit as

$$B_{nl} = \frac{16^{l+1}l(2l-1)\Gamma(2l-1)^2\Gamma(l+n+1)^2}{n^{4l+8}(l+1)\Gamma(l+1)^4\Gamma(4l+3)\Gamma(n-l)^2}. \quad (5)$$

However, we caution the reader that numerical analysis shows that (5) underestimates the depletion power by approximately one order of magnitude (Yoshino and Kodama 2014; Brito et al. 2015a). The scaling powers of M_{nlm} and α , in contrast, are robust for $\alpha \ll 1$. Nevertheless, due to its analytical generality for all n and l , we will adopt (5) to estimate the depletion time scale,

$$T_{nlm}^{(\text{deplete})} \approx B_{nl}^{-1} \frac{M_B^2}{M_{nlm,0}^2} \alpha^{-4l-10}, \quad (6)$$

and warn the reader about the potential $\mathcal{O}(10)$ uncertainty due to (5). Here $M_{nlm,0}$ is the initial mass of the cloud state, whose value at saturation can be estimated

² Throughout this paper, we assume the ultralight boson is a (pseudo)scalar.

using angular momentum conservation (see Table. 1 in [Baumann et al. \(2020\)](#)).

Now let us come to the binary system case. The motion of a binary companion will generate a periodic tidal perturbation on the gravitational atom, leading to level crossings in the atomic spectrum. At a large binary separation, the tidal perturbation is solely dependent on the mass of the binary companion. Thus it can be any astronomical object compact enough to fit into the orbit. In particular, we consider a pulsar of mass M_P . GCP transitions happen when the frequency of pulsar revolution matches the energy difference between two atomic states. After expanding the tidal perturbation into multipole moments and calculating its matrix elements between atomic states, one obtains the following selection rule for a process $|nlm\rangle \rightarrow |n'l'm'\rangle$ ([Baumann et al. 2019a](#)):

$$\begin{aligned} -m' + m_* + m &= 0 \\ l + l_* + l' &= 2p, \text{ for } p \in \mathbb{Z} \\ |l - l'| &\leq l_* \leq l + l' \end{aligned} \quad (7)$$

For large circular equatorial orbits, the resonance period is

$$P_r = 2\pi \left| \frac{\Delta m}{\Delta E} \right|, \quad (8)$$

with $\Delta E \equiv E_{n'l'm'} - E_{nlm}$, $\Delta m \equiv m' - m$. We see that a larger ΔE generically corresponds to shorter orbital periods.

The atomic transition produces backreaction to the binary, resulting in floating orbit and sinking orbit. We call transition with $\Delta E < 0$ floating orbit, where the boson cloud loses its energy, delaying the orbital decay. In contrast, $\Delta E > 0$ gives sinking orbit, where the period of binary system decreases faster with their energy given to the cloud. The total transition time is $\Delta t_{\text{tot}} = \Delta t + \Delta t_c$, where Δt is the transition time without backreaction, and Δt_c is the extra time caused by the backreaction. Here Δt_c is positive for floating orbits and is negative for sinking orbits. The detailed expressions of Δt and Δt_c can be found in ([Baumann et al. 2020](#)). A GCP transition can sometimes turn a superradiant state into a non-superradiant state with negative $\Gamma_{n'l'm'}$, where the cloud is absorbed into the BH. Interestingly, it is recently pointed out this may be avoided under certain conditions ([Takahashi and Tanaka 2021](#)).

3. Bohr transitions vs fine and hyperfine transitions

For Bohr transitions among the lowest few states, the energy difference is typically large, hence a short binary period. For instance, a Bohr transition from $n = 3$ to $n = 2$ gives a resonance period

$$P_{3 \rightarrow 2} = \frac{288GM_B}{5\alpha^3} = (2.6 \text{ s}) \times \left(\frac{M_B}{5M_\odot} \right) \left(\frac{\alpha}{0.12} \right)^{-3}. \quad (9)$$

Denoting $q \equiv \frac{M_P}{M_B}$, the time left until the merger is then

$$T_{3 \rightarrow 2}^{(\text{merger})} = (1 \text{ day}) \times \frac{(1+q)^{1/3}}{q} \left(\frac{M_B}{5M_\odot} \right) \left(\frac{\alpha}{0.12} \right)^{-8}, \quad (10)$$

suggesting that the PSR-BH binary is near the end of the inspiral phase. Although the orbital decay at this stage is significant for both pulsar timing and GW detectors, the likelihood of encountering a binary at this stage is smaller than that in the middle of the inspiral phase by at least several orders of magnitude. Yet the total number of observable PSR-BH binaries in our Galaxy is estimated to be $\mathcal{O}(10^2\text{-}10^3)$ ([Faucher-Giguère and Loeb 2011](#); [Shao and Li 2018](#); [Chattopadhyay et al. 2020](#)). Therefore, the event rate for Bohr transitions may be extremely low.

Another problem for Bohr transitions comes from the validity of multipole expansion. The binary separation for a typical $n = 3$ to $n = 2$ Bohr transition is

$$R_{3 \rightarrow 2} = (4.8 \times 10^3 \text{ km}) \times (1+q)^{1/3} \left(\frac{M_B}{5M_\odot} \right) \left(\frac{\alpha}{0.12} \right)^{-2}. \quad (11)$$

The size of the bosonic cloud for the state with principal quantum number n is $r_n = n^2 r_1$, with $r_1 = M_B \alpha^{-2}$ being the Bohr radius. For $n = 3$, we have

$$r_3 = 9M_B \alpha^{-2} = (4.6 \times 10^3 \text{ km}) \left(\frac{M_B}{5M_\odot} \right) \left(\frac{\alpha}{0.12} \right)^{-2}. \quad (12)$$

Hence the multipole expansion, in particular, the narrow resonance approximation of the $l_* = m_* = 2$ quadrupole moment ([Baumann et al. 2020](#)) may be questionable for $q \sim 1$. This is because when $R_{3 \rightarrow 2}$ is close to r_3 , the pulsar is already moving inside the cloud, and higher multipole moments that mediate other transitions with $|\Delta m| > 2$ are non-negligible. In addition, the dynamical friction of the cloud ([Zhang and Yang 2020](#)), upscattering effects ([Wong 2020](#)) and the formation of molecular states ([Ikeda et al. 2021](#)) can also have important impacts on the transition. As a result, an accurate account for Bohr transitions may require a non-perturbative treatment.

For fine ($\Delta n = 0, \Delta l \neq 0$) and hyperfine ($\Delta n = \Delta l = 0, \Delta m \neq 0$) transitions, however, both difficulties can be evaded. From (2), we see that the energy difference in a fine (hyperfine) transition is smaller by a factor of α^2 (α^3) than a Bohr transition, leading to a much longer resonance period. This means they can happen for PSR-BH binaries in the middle phase of inspiral, which is statistically more favored. The binary separation is also enlarged by a factor of $\alpha^{-4/3}$ (α^{-2}) for a fine (hyperfine) transition, making the multipole expansion well-defined and the $|\Delta m| = m_* = 2$ approximation accurate.

Moreover, for $n \leq 3$, fine/hyperfine transitions always occur with $\Delta E < 0$. This is because the initial cloud state has maximal helicity and the highest energy within the same l -multiplet, and the excitation to a higher l -multiplet is forbidden for $n \leq 3$. This suggests that these phenomenologically interesting fine/hyperfine transitions give rise to floating orbits. Thus the time spent on the GCP resonance is extended by Δt_c , further increasing the likelihood of detection. If $\Delta t_c \gg \Delta t \gtrsim T^{(\text{deplete})}$, once the binary hits the resonance band, the pulsar will be stuck on the floating orbit until the cloud depletes, which typically takes 10^8 yr. This greatly enhances the detection likelihood.

A quantitative comparison of Bohr transitions and fine/hyperfine transitions is shown in TABLE. 1, where

TABLE 1
A COMPARISON BETWEEN BOHR TRANSITIONS AND FINE/HYPERFINE TRANSITIONS

	Transition	P_r (hr)	Δt (yr)	Δt_c (yr)	r_n/R_r	$T^{(\text{growth})}$ (yr)	$T^{(\text{deplete})}$ (yr)	$T^{(\text{merge})}$ (yr)
Bohr	$ 322\rangle \rightarrow 200\rangle$	6.4×10^{-4}	2.8×10^{-3}	2.2×10^{-3}	0.96	9600	10^{13}	7.9×10^{-3}
	$ 322\rangle \rightarrow 100\rangle$	9.9×10^{-5}	1.9×10^{-5}	2.8×10^{-5}	3.3	9570	10^{13}	5.5×10^{-5}
	$ 311\rangle \rightarrow 21-1\rangle$	7.0×10^{-4}	3.6×10^{-3}	1.4×10^{-2}	0.89	4.7×10^{-2}	10^5	1.0×10^{-2}
	$ 211\rangle \rightarrow 31-1\rangle$	7.1×10^{-4}	3.6×10^{-3}	-1.4×10^{-2}	0.89	1.7×10^{-2}	10^5	1.0×10^{-2}
Fine	$ 322\rangle \rightarrow 300\rangle$	1.9×10^{-2}	25	6.3	9.8×10^{-2}	9600	10^{13}	72
Hyperfine	$ 322\rangle \rightarrow 320\rangle$	12	7.5×10^8	2.2×10^7	1.3×10^{-3}	9600	10^{13}	2.1×10^9
	$ 321\rangle \rightarrow 32-1\rangle$	6.4	1.3×10^8	2.4×10^7	2.0×10^{-3}	6.4×10^5	10^5-10^{13}	3.8×10^8
	$ 311\rangle \rightarrow 31-1\rangle$	1.3	1.8×10^6	5.6×10^5	6.0×10^{-3}	4.7×10^{-2}	10^5	5.1×10^6
	$ 211\rangle \rightarrow 21-1\rangle$	0.38	7.0×10^4	3.3×10^4	6.0×10^{-3}	1.7×10^{-2}	10^5	2.0×10^5

the mass parameters are fixed to be $\alpha = 0.12$, $M_B = 5M_\odot$ and $M_P = 1.4M_\odot$. Here we have enumerated all GCP transitions that involve states with $n, n' \leq 3$, and that are mediated by the $l_* = m_* = 2$ quadrupole moment. Because of the uncertainty in the $T^{(\text{deplete})}$ formula (6), we have only kept its order of magnitude. Also note that the depletion time for the state $|321\rangle$ has not yet been computed in the literature to our best knowledge. Therefore, we only give its possible range estimated by $T_{322}^{(\text{deplete})}$ and $T_{311}^{(\text{deplete})}$. It is clear from TABLE 1 that fine/hyperfine transitions solve all issues aforementioned, by having a much larger P_r , a much longer Δt , $T^{(\text{merger})}$, and a much smaller ratio r_n/R_r .

Going beyond the lowest a few states, we can find more interesting structures emerging. Given the $l_* = m_* = |\Delta m| = 2$ constraint and the selection rules (7), one can find all possible quadrupole-mediated GCP transitions with $n, n' \leq n_{\text{max}}$. The formula for the total number of allowed transitions is

$$N_{\text{tot}, n_{\text{max}}}^{(B/F/HF)} = \frac{1}{2} (n_{\text{max}} - 2) n_{\text{max}} (n_{\text{max}}^2 - 2n_{\text{max}} + 3), \quad (13)$$

where $n_{\text{max}} \geq 4$. Within the n -th energy level, the number of allowed fine transitions and hyperfine transitions are given by

$$\begin{aligned} N_n^{(F)} &= 2n^2 - 10n + 14 \\ N_n^{(HF)} &= n^2 - 3n + 3, \text{ with } n \geq 4. \end{aligned} \quad (14)$$

We have enumerated all allowed transitions with $n_{\text{max}} = 4$ and $n_{\text{max}} = 8$ in FIG. 4. The transition graph with $n_{\text{max}} \geq 4$ neatly factorize into the direct product of four connected subgraphs. This can be understood as the consequence of the quadrupole approximation. Because $\Delta m = 2$, states with odd m cannot jump to states with even m' , vice versa. In addition, parity conservation further divides these two sets into parity-odd (odd l and l') families and parity-even (even l and l') families, leading to the four disjoint sectors. Note that although higher multipole moments ($l_* \geq 3$) are able to mediate Bohr transitions between these sectors, they are in general too small to influence fine/hyperfine transitions.

The advantage of fine/hyperfine transitions over Bohr transitions persists as more GCP transitions are included. In FIG. 1, we have shown the time left until merger as well as the ratio of cloud size and binary separation for all transitions up to $n_{\text{max}} = 10$. It is clear that the three types of transitions occupy differ-

ent regions in the parameter space. Most Bohr transitions lie in the gray region where the multipole expansion breaks down, while fine/hyperfine transitions are far safer. Fine/hyperfine transitions also correspond to a much longer time before merger, hence a higher event rate.

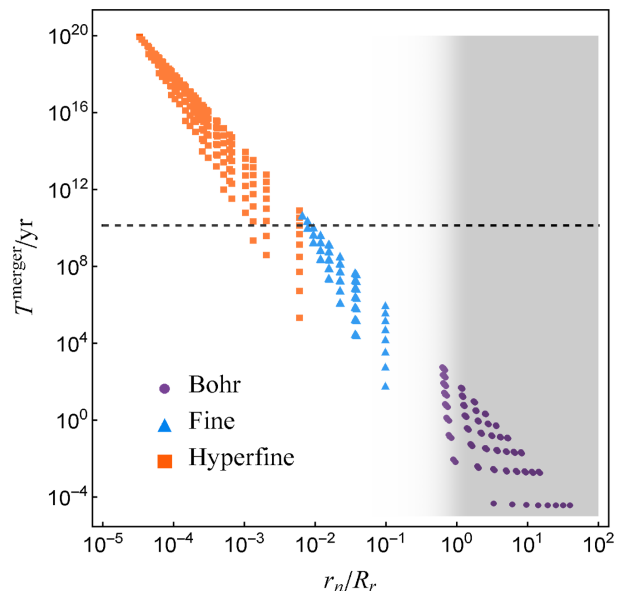


FIG. 1.— The distribution of Bohr/fine/hyperfine transitions in the parameter space spanned by the time T^{merger} left until merger as well as the ratio of cloud size and binary separation r_n/R_r . Here we have considered all quadrupole-mediated GCP transitions up to $n_{\text{max}} = 10$. There are in total $N_{\text{tot}, 10}^{(B/F/HF)} = 3320$ transitions. The parameters are again chosen as $\alpha = 0.12$, $M_B = 5M_\odot$ and $M_P = 1.4M_\odot$. The gray region is where the multipole expansion and narrow resonance approximation break down. The dashed line represents the age of the universe. A smaller ratio r_n/R_r gives better quadrupole approximation and a longer T^{merger} enhances the event rate^a. Hence the advantage of fine/hyperfine transitions over Bohr transitions is obvious.

^aNotice that a T^{merger} longer than the age of the universe does not mean the transition cannot happen, nor the binary does not exist. It just means that the binary is going to spend an extremely long time in the inspiral phase.

4. Uncovering fine and hyperfine structures: Pulsar timing accuracy

The direct observation of GCP transitions for a PSR-BH binary relies on an accurate measurement of orbital motion, which is recorded as modulations in the Rømer delay of pulsar time-of-arrivals. Unlike Bohr transitions, fine/hyperfine transitions occur at a much longer orbital period, where the GW emission is still weak. The resonance frequency lies in the range of the space-based GW detectors such as LISA. At a low orbital frequency, the corresponding orbital decay is much slower. Such a weak effect may require a long-term observation that lasts more than a decade. As a comparison, LISA only has a lifetime of 4–6 years (Amaro-Seoane et al. 2017). Therefore, it is questionable whether the first generation of space GW detectors (Amaro-Seoane et al. 2017; Luo et al. 2020; Mei et al. 2021; Ando et al. 2009) are precise enough to probe the GCP transitions in due time. In contrast, radio telescopes are earth-based and can last many decades. For instance, the Arecibo telescope built in 1963 had been functioning for 57 years before its tragic collapse in 2020. Thus a long-term observation of a PSR-BH binary may reveal the tiny deviations of orbital decay and uncover the fine/hyperfine structure of the gravitational atom.

The orbital decay of the PSR-BH binary, according to Hulse and Taylor (1975) and Weisberg and Taylor (2004), can be observed by recording the periastron time shift

$$\Delta_P = t - P(0) \int_0^t \frac{1}{P(t')} dt'. \quad (15)$$

If we consider a small timescale with respect to that of a significant orbital decay, we can linearize the period change by $P(t) \simeq P(0) + \dot{P}t$. The periastron time shift then increases quadratically with observation time:

$$\Delta_P = \frac{1}{2} \frac{\dot{P}}{P} t^2. \quad (16)$$

Under the influence of isolated atomic transitions, the orbital decay due to GW emission can be approximated as (Ding et al. 2021)

$$\begin{aligned} \dot{P} = & -\frac{96}{5} (2\pi)^{8/3} (GM_B)^{5/3} \frac{q}{(1+q)^{1/3}} P^{-5/3} \\ & \times \frac{1}{1 \pm \frac{\Delta t_c}{\Delta t} \times \Pi\left(\frac{P-P_r}{\Delta P_r}\right)}, \end{aligned} \quad (17)$$

where Π is the Heaviside-Pi window function that characterize the bandwidth of the GCP resonance, *i.e.*, $\Delta P_r \simeq \frac{0.6q}{1+q} P_r$. The deviation of $P(t)$ and hence $\Delta_P(t)$ from the general relativity prediction will be the signal that we are after.

In order to successfully detect GCP resonances, we need to ensure that the uncertainty σ_{Δ_P} is smaller than total Periastron time shift Δ_P . Notice that the periastron time shift is not measured from its definition (15), which demands an accurate measurement of the orbital period as a function of time. Rather, we measure the periastron time shift directly by counting the accumu-

lated orbital periods. We determine one orbital period by counting the number of pulses between two pulses with equal Rømer delay and equal time derivative of Rømer delay. In order to resolve an orbital period, the maximal Rømer delay must be larger than the pulse width w , which is on a similar order as the pulse period τ . Therefore, we demand

$$\frac{2R_r}{1+q} > \tau, \quad (18)$$

which automatically implies $P_r > \tau$. The error during one continuous observation window is also $w \sim \tau$. Suppose we can observe the pulsar for t_{obs} every day, which means we can measure t_{obs}/P periods every day. That is, for every single continuous measurement, the error can be estimated by $\frac{\tau}{\min(t_{obs}, t)/P}$. If we observe for $0 < t \leq T_{obs}$, where T_{obs} is the maximal observation time, then the number of independent measurement is $\lceil t/1 \text{ day} \rceil$, where $\lceil \cdot \rceil$ is ceil function. In summary, the uncertainty for Periastron time shift is

$$\sigma_{\Delta_P} = \frac{1}{\sqrt{\lceil t/1 \text{ day} \rceil}} \frac{\tau}{\min(t_{obs}, t)/P}. \quad (19)$$

We can detect the GCP transitions only if the difference between the periastron time shift with transition backreaction and that without it is greater than the observation uncertainty,

$$|\Delta_P|_{GCP} - \Delta_P|_{GR} > \sigma_{\Delta_P}. \quad (20)$$

In addition, there are two more constraints on the model parameters. Namely, the superradiant time scale of boson cloud should be short enough to observe, and the cloud should be stable on an astrophysical timescale (Baumann et al. 2020),

$$T^{(\text{growth})} \lesssim 10^6 \text{ yrs}, T^{(\text{deplete})} \gtrsim 10^8 \text{ yrs}. \quad (21)$$

Combining the constraints (18), (20) and (21), we obtain the feasible parameter region for the fine/hyperfine transitions³ shown in FIG. 2. Overall, transitions starting with $|322\rangle$ give a wide range of parameter region that covers $10^{-3} M_\odot < M_B < 10^8 M_\odot$ and $0.06 < \alpha < 0.5$. In contrast, transitions starting with $|311\rangle$ and $|211\rangle$ allow a relatively limited parameter space with significantly smaller α . Notice that the right edge of the parameter space is constrained by the depletion time, which is subjected to an $\mathcal{O}(10)$ uncertainty. The lower edge is constrained by the Rømer delay resolvability (18). The upper edge is constrained by the timing accuracy of periastron time deviation (20). The left edge is either constrained by the timing accuracy (for hyperfine transitions) or the cloud growth time (for fine transitions).

Thus we see that timing accuracy plays an important role in probing hyperfine transitions. Naturally, pulsars with shorter rotations period τ provide a finer resolution of the orbital motion, thereby increasing the timing accuracy. Alternatively, for a given PSR-BH system, one can also extend the observation time T_{obs} to increase the timing accuracy. This fact is demonstrated in FIG. 3 for the hyperfine transition $|322\rangle \rightarrow |320\rangle$. Some parameter

³ Note that the transition $|321\rangle \rightarrow |32-1\rangle$ is not shown due to our lack of information on $T_{321}^{(\text{deplete})}$.

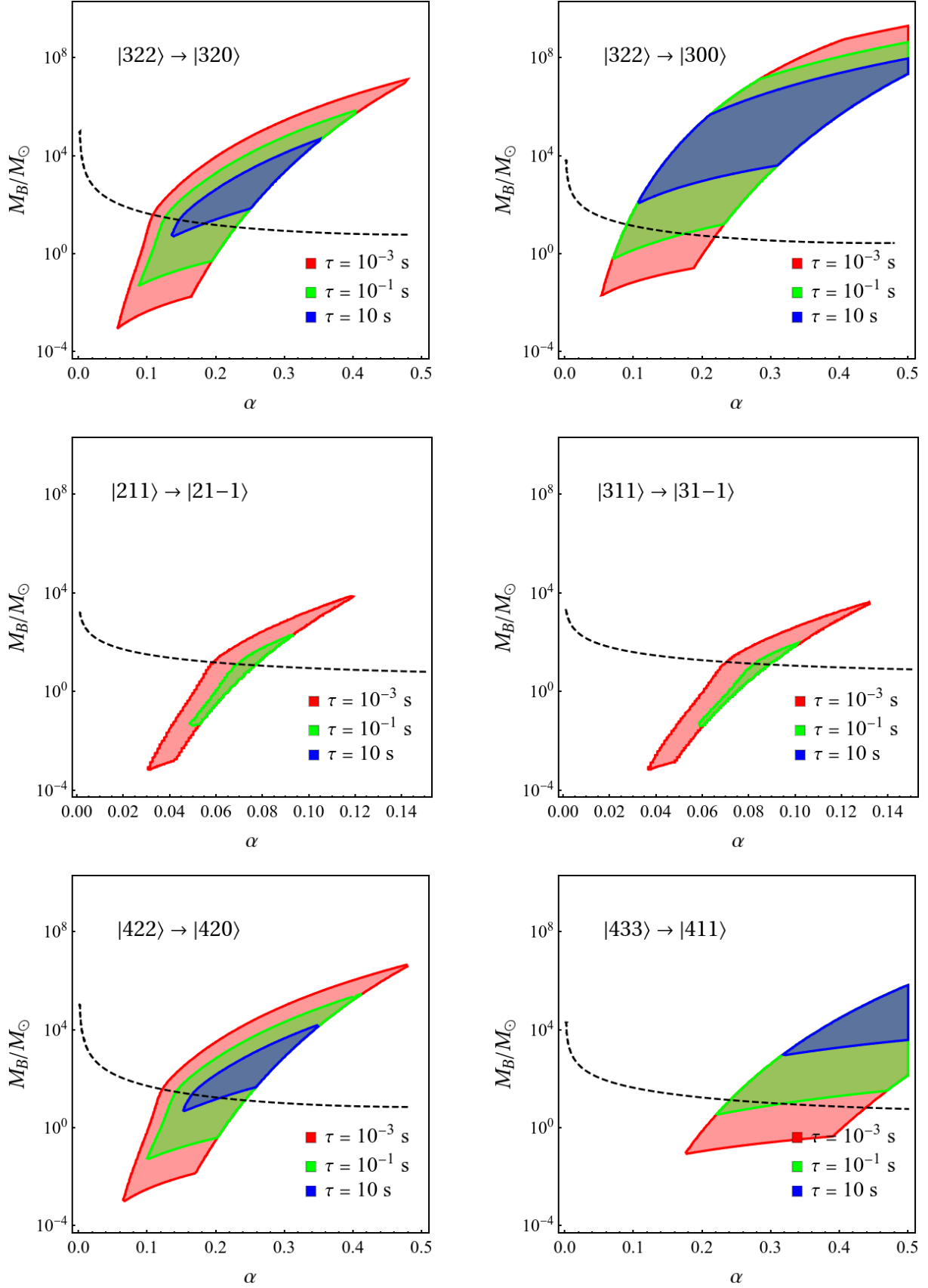


FIG. 2.— The feasible regions for α , M_B and different pulsar periods τ . Here we have taken the mass of the pulsar to be $M_P = 1.4M_\odot$ and assumed an observation time $T_{obs} = 1$ decade. The black dashed line given by $\Delta t = \Delta t_c$ divides the parameter space into the upper half with strong backreaction and the lower half with weak backreaction. The timing accuracy edge acquires a turning point near this line because the periastron time shift has different asymptotic behaviors across the line.

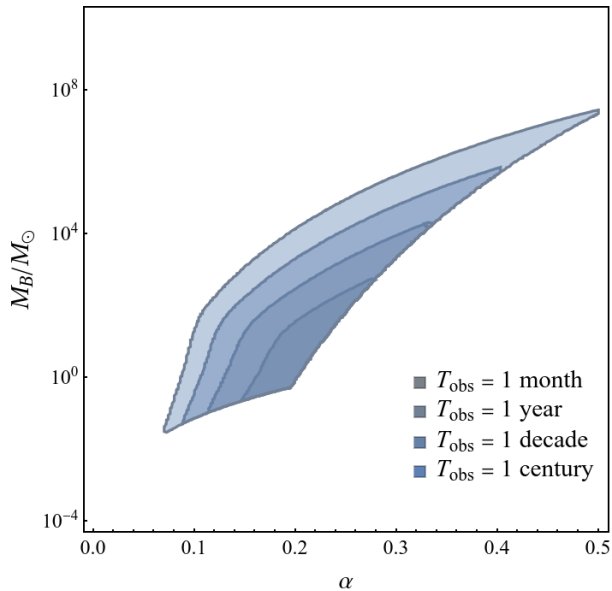


FIG. 3.— The feasible parameter space for α , M_B and different observe time T_{obs} for the hyperfine transition $|322\rangle \rightarrow |320\rangle$. Here we have chosen $M_P = 1.4M_\odot$ and $\tau = 0.1\text{s}$.

choices may require decades of observation for a clear detection, a task suitable only for ground-based apparatus such as radio telescopes.

The fine/hyperfine transitions for states with $n \geq 4$ are qualitatively similar. Since the superradiance growth rate and the GW depletion rate is not very sensitive to the principal quantum number, the feasible parameter regions for $|n22\rangle \rightarrow |n20\rangle$ and $|n22\rangle \rightarrow |n00\rangle$ are similar to that plotted in FIG. 2. Transitions starting with higher angular quantum number l generally require a larger α , since their growth rate are further suppressed by powers of α .

5. Conclusion

In this paper, we focused on probing fine/hyperfine GCP transitions in a PSR-BH binary with pulsar timing. Starting from a general review of the gravitational atom and GCP, we pointed out the problems faced by Bohr transitions. Namely, the Bohr transitions may be extremely rare because they happen near the end of the inspiral phase. The quadrupole narrow resonance approximation may also become invalid when the binary separation is comparable to the cloud size. Then we showed that these problems can be evaded in the fine/hyperfine transitions, which typically enjoy a longer resonance period and a greater binary separation. All fine/hyperfine transitions with $n \leq 3$ lead to floating orbits that delay the orbital decay, further enhancing the likelihood of observation. The advantage persists for higher energy levels, as the three types of transitions occupy distinct regions in the parameter space. The subsequent analysis of pulsar timing accuracy demonstrates the feasibility of detecting fine/hyperfine transitions in GCP. In particular, we find that the fine transition $|n22\rangle \rightarrow |n00\rangle$ and hyperfine transitions $|n22\rangle \rightarrow |n20\rangle$ give wide parameter regions that can be probed via pulsar timing. Increasing

the total observation time also increases the timing accuracy, making the detection of transitions with large black hole mass possible. In the spirit of multi-messenger astronomy, due to the long lifetime of radio telescopes and the stringent accuracy requirement, the observation of fine/hyperfine transitions via this PSR-BH-radio channel should serve as a complement to observing Bohr transitions via the BH-BH-GW channel.

However, there are still many questions left unanswered in the current work, and we hope to address them in the future. We conclude this paper by mentioning a few of them. First, our estimation of boson cloud depletion time is based on an approximate formula with a considerable amount of error, especially at large α and when $l \neq m$. We hope to improve our constraints in the future using more accurate numerical solutions of cloud depletion. Second, we have argued that the event rate of fine/hyperfine transitions is greatly enhanced by their long orbital periods and floating orbits, yet we did not give any explicit estimation of the likelihood of observation. To perform such an analysis, one needs to consider the initial distribution of BHs and pulsars in the Galaxy as well its evolution history. Third, in addition to pulsar timing, the measurement of the Doppler effect and the ellipsoidal modulation of a White Dwarf (WD) in a binary is nowadays accurate enough for detecting the orbital decay (Hermes et al. 2012; Burdge et al. 2019a,b). Since there are more WDs than pulsars in the Galaxy, it is interesting to consider probing GCP resonances in WD-BH binaries, whose event rate can be further enhanced. We can also consider the Doppler effect of a generic Neutron Star (NS) which may not necessarily be a pulsar. This possibility becomes more exciting after the recent LIGO-Virgo discovery of two NS-BH mergers by Abbott et al. (2021). The question is, of course, whether the accuracy can reach the requirement of detecting the *deviations* in the orbital decay due to GCP resonances. We leave a detailed analysis to future works.

Acknowledgment

We would like to thank Qianhang Ding and Chon Man Sou for helpful discussions. This work was supported in part by the CRF grant C6017-20GF by the RGC of Hong Kong SAR, and the NSFC Excellent Young Scientist (EYS) Scheme (Hong Kong and Macau) Grant No. 12022516.

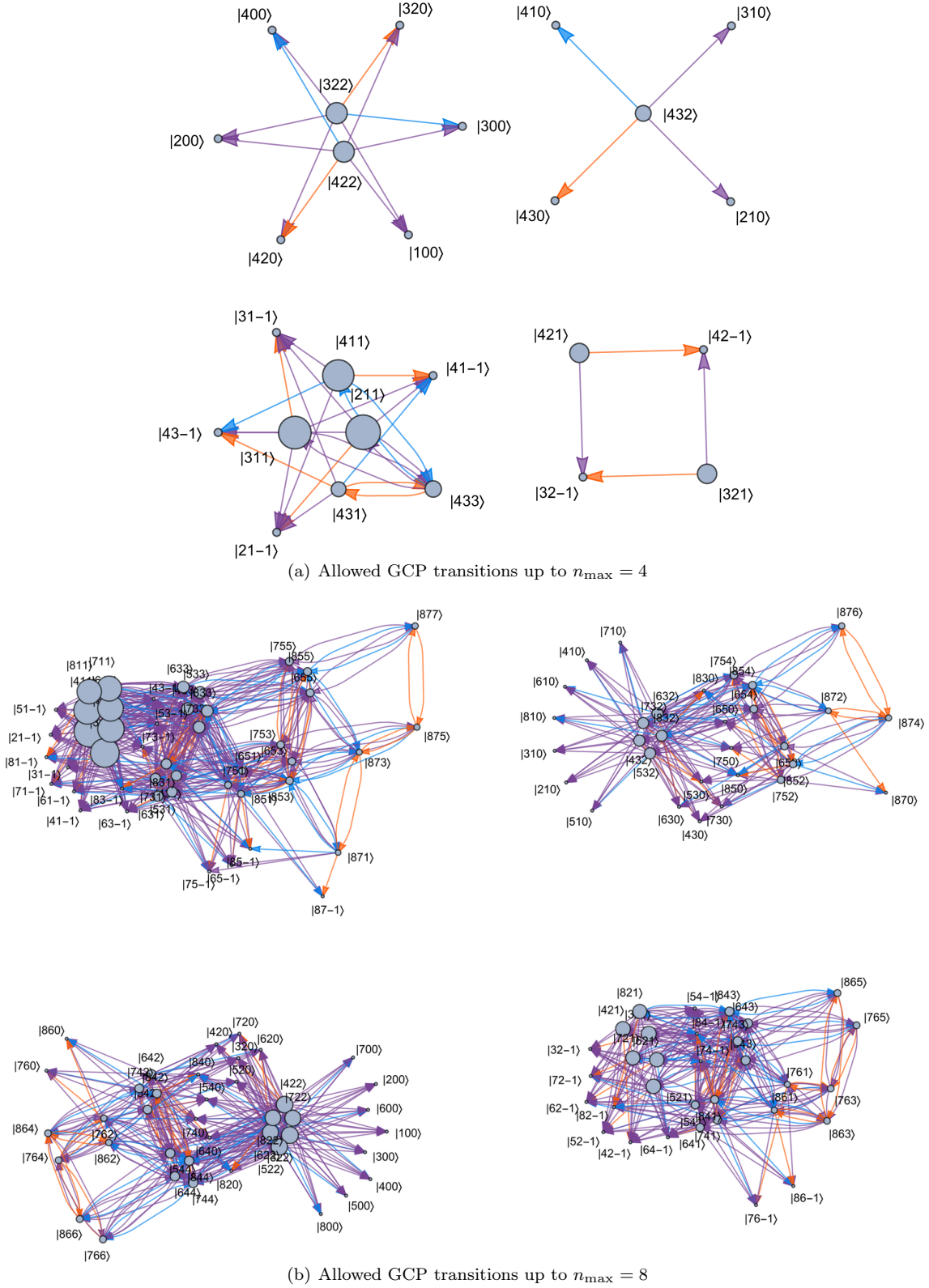


FIG. 4.— The transition graph for states with $n, n' \leq n_{\max}$. The purple, blue and orange arrows represent Bohr transitions, fine transitions and hyperfine transitions, respectively. The size of the vertices indicates the superradiance growth rate, *i.e.*, a large vertex corresponds to a fast-growing cloud.

REFERENCES

- Abbott, R. et al. (2021). Observation of Gravitational Waves from Two Neutron Star–Black Hole Coalescences. *Astrophys. J. Lett.*, 915(1):L5.
- Amaro-Seoane, P., Audley, H., Babak, S., Baker, J., Barausse, E., Bender, P., Berti, E., Binetruy, P., Born, M., Bortoluzzi, D., et al. (2017). Laser interferometer space antenna. *arXiv preprint arXiv:1702.00786*.
- Ando, M., Kawamura, S., Sato, S., Nakamura, T., Tsubono, K., Araya, A., Funaki, I., Ioka, K., Kanda, N., Moriwaki, S., et al. (2009). Decigo pathfinder. *Classical and quantum gravity*, 26(9):094019.
- Angéil, R., Saha, P., and Merritt, D. (2010). Toward relativistic orbit fitting of galactic center stars and pulsars. *The Astrophysical Journal*, 720(2):1303.
- Arvanitaki, A. and Dubovsky, S. (2011). Exploring the String Axiverse with Precision Black Hole Physics. *Phys. Rev. D*, 83:044026.
- Arzoumanian, Z., Baker, P. T., Blumer, H., Bécsy, B., Brazier, A., Brook, P. R., Burke-Spolaor, S., Chatterjee, S., Chen, S., Cordes, J. M., et al. (2020). The nanograv 12.5 yr data set: Search for an isotropic stochastic gravitational-wave background. *The Astrophysical Journal Letters*, 905(2):L34.
- Baumann, D., Chia, H. S., and Porto, R. A. (2019a). Probing ultralight bosons with binary black holes. *Physical Review D*, 99(4):044001.
- Baumann, D., Chia, H. S., Porto, R. A., and Stout, J. (2020). Gravitational collider physics. *Physical Review D*, 101(8):083019.
- Baumann, D., Chia, H. S., Stout, J., and ter Haar, L. (2019b). The spectra of gravitational atoms. *Journal of Cosmology and Astroparticle Physics*, 2019(12):006.
- Becker, W., Bernhardt, M. G., and Jessner, A. (2013). Autonomous spacecraft navigation with pulsars. *arXiv preprint arXiv:1305.4842*.
- Brito, R., Cardoso, V., and Pani, P. (2015a). Black holes as particle detectors: evolution of superradiant instabilities. *Class. Quant. Grav.*, 32(13):134001.
- Brito, R., Cardoso, V., and Pani, P. (2015b). *Superradiance: Energy Extraction, Black-Hole Bombs and Implications for Astrophysics and Particle Physics*, volume 906. Springer.
- Burdge, K. B., Coughlin, M. W., Fuller, J., Kupfer, T., Bellm, E. C., Bildsten, L., Graham, M. J., Kaplan, D. L., Van Roestel, J., Dekany, R. G., et al. (2019a). General relativistic orbital decay in a seven-minute-orbital-period eclipsing binary system. *Nature*, 571(7766):528–531.
- Burdge, K. B., Fuller, J., Phinney, E. S., Van Roestel, J., Claret, A., Cukanovaite, E., Fusillo, N. P. G., Coughlin, M. W., Kaplan, D. L., Kupfer, T., et al. (2019b). Orbital decay in a 20 minute orbital period detached binary with a hydrogen-poor low-mass white dwarf. *The Astrophysical Journal Letters*, 886(1):L12.
- Camenzind, M. (2007). *Compact objects in astrophysics : white dwarfs, neutron stars, and black holes*.
- Cardoso, V., Dias, O. J. C., Lemos, J. P. S., and Yoshida, S. (2004). The Black hole bomb and superradiant instabilities. *Phys. Rev. D*, 70:044039. [Erratum: Phys.Rev.D 70, 049903 (2004)].
- Chattopadhyay, D., Stevenson, S., Hurley, J. R., Bailes, M., and Broekgaarden, F. (2020). Modelling Neutron Star–Black Hole Binaries: Future Pulsar Surveys and Gravitational Wave Detectors.
- Damour, T., Deruelle, N., and Ruffini, R. (1976). On Quantum Resonances in Stationary Geometries. *Lett. Nuovo Cim.*, 15:257–262.
- Detweiler, S. L. (1980). KLEIN-GORDON EQUATION AND ROTATING BLACK HOLES. *Phys. Rev. D*, 22:2323–2326.
- Dewdney, P. E., Hall, P. J., Schilizzi, R. T., and Lazio, T. J. L. (2009). The square kilometre array. *Proceedings of the IEEE*, 97(8):1482–1496.
- Ding, Q., Tong, X., and Wang, Y. (2021). Gravitational collider physics via pulsar–black hole binaries. *The Astrophysical Journal*, 908(1):78.
- Faucher-Giguère, C.-A. and Loeb, A. (2011). Pulsar-black hole binaries in the galactic centre. *Monthly Notices of the Royal Astronomical Society*, 415(4):3951–3961.
- Hawking, S. W. (1974). Black hole explosions. *Nature*, 248:30–31.
- Hawking, S. W. (1975). Particle Creation by Black Holes. *Commun. Math. Phys.*, 43:199–220. [Erratum: Commun.Math.Phys. 46, 206 (1976)].
- Hawking, S. W., Perry, M. J., and Strominger, A. (2016). Soft Hair on Black Holes. *Phys. Rev. Lett.*, 116(23):231301.
- Hermes, J., Kilic, M., Brown, W. R., Winget, D., Prieto, C. A., Gianninas, A., Mukadam, A. S., Cabrera-Lavers, A., and Kenyon, S. J. (2012). Rapid orbital decay in the 12.75-minute binary white dwarf j0651+ 2844. *The Astrophysical Journal Letters*, 757(2):L21.
- Hobbs, G. et al. (2010). The international pulsar timing array project: using pulsars as a gravitational wave detector. *Class. Quant. Grav.*, 27:084013.
- Hulse, R. A. and Taylor, J. H. (1975). Discovery of a pulsar in a binary system. *The Astrophysical Journal*, 195:L51–L53.
- Ikeda, T., Bernard, L., Cardoso, V., and Zilhao, M. (2021). Black hole binaries and light fields: Gravitational molecules. *Physical Review D*, 103(2):024020.
- Kavic, M., Liebling, S. L., Lippert, M., and Simonetti, J. H. (2020). Accessing the axion via compact object binaries. *Journal of Cosmology and Astroparticle Physics*, 2020(08):005.
- Konoplya, R. A. and Zhidenko, A. (2011). Quasinormal modes of black holes: From astrophysics to string theory. *Rev. Mod. Phys.*, 83:793–836.
- Landau, L. D. (1932). Zur theorie der energieubertragung ii. *Z. Sowjetunion*, 2:46–51.
- Luo, Z., Guo, Z., Jin, G., Wu, Y., and Hu, W. (2020). A brief analysis to taiji: Science and technology. *Results in Physics*, 16:102918.
- Mei, J., Bai, Y.-Z., Bao, J., Barausse, E., Cai, L., Canuto, E., Cao, B., Chen, W.-M., Chen, Y., Ding, Y.-W., et al. (2021). The tianqin project: current progress on science and technology. *Progress of Theoretical and Experimental Physics*, 2021(5):05A107.
- Ng, K. K. Y., Isi, M., Haster, C.-J., and Vitale, S. (2020). Multiband gravitational-wave searches for ultralight bosons. *Phys. Rev. D*, 102(8):083020.
- Nielsen, A. B. (2016). On the distribution of stellar-sized black hole spins. *J. Phys. Conf. Ser.*, 716(1):012002.
- O’Shaughnessy, R. W., Kaplan, J., Kalogera, V., and Belczynski, K. (2005). Bounds on expected black hole spins in inspiraling binaries. *Astrophys. J.*, 632:1035–1041.
- Penrose, R. (1969). Gravitational collapse: The role of general relativity. *Riv. Nuovo Cim.*, 1:252–276.
- Press, W. H. and Teukolsky, S. A. (1972). Floating Orbits, Superradiant Scattering and the Black-hole Bomb. *Nature*, 238:211–212.
- Seymour, B. C. and Yagi, K. (2020). Probing massive scalar and vector fields with binary pulsars. *Physical Review D*, 102(10):104003.
- Shao, Y. and Li, X.-D. (2018). Black Hole/Pulsar Binaries in the Galaxy. *Mon. Not. Roy. Astron. Soc.*, 477(1):L128–L132.
- Shapiro, S. L. and Teukolsky, S. A. (1983). *Black holes, white dwarfs, and neutron stars: The physics of compact objects*.
- Takahashi, T. and Tanaka, T. (2021). Axion clouds may survive the perturbative tidal interaction over the early inspiral phase of black hole binaries.
- Weisberg, J. M. and Taylor, J. H. (2004). Relativistic binary pulsar b1913+ 16: Thirty years of observations and analysis. *arXiv preprint astro-ph/0407149*.
- Wong, L. K. (2020). Evolution of diffuse scalar clouds around binary black holes. *Phys. Rev. D*, 101(12):124049.
- Yoshino, H. and Kodama, H. (2014). Gravitational radiation from an axion cloud around a black hole: Superradiant phase. *Progress of Theoretical and Experimental Physics*, 2014(4):043E02.
- Zel’Dovich, Y. B. (1971). Generation of Waves by a Rotating Body. *Soviet Journal of Experimental and Theoretical Physics Letters*, 14:180.
- Zener, C. (1932). Nonadiabatic crossing of energy levels. *Proc. Roy. Soc. Lond. A*, 137:696–702.
- Zhang, J. and Yang, H. (2020). Dynamic signatures of black hole binaries with superradiant clouds. *Physical Review D*, 101(4):043020.